In preparation for submission to *Solar Physics*
http://www.springerlink.com/content/0038-0938

Cross-Calibration of SMART-1 XSM with GOES and RHESSI

Mikko Väänänen · Lauri Alha · Juhani Huovelin

submitted: 28 April 2009; accepted: 15 September 2009

Abstract A number of X-ray instruments have been active in observing the solar coronal X-ray radiation this decade. We have compared XSM observations with simultaneous GOES and RHESSI observations. We present flux calibrations for all instruments, and compare XSM and GOES total emission measures (TEM) and temperatures (T).

The model-independent flux comparison with XSM and GOES data at the $1-8$ Å band shows that the fluxes agree with a ratio of 0.94 ± 0.09 for the data up to April 2005. The Mewe model-dependent Ts and TEMs differ as XSM observes 1.47 ± 0.03 times higher Ts than GOES and 1.23 ± 0.08 times higher TEMs and 0.92 ± 0.05 times lower fluxes. The comparison with RHESSI data at the $6-8$ keV band shows that the average XSM/RHESSI flux ratio is 2.63 ± 0.23. The discrepancies revealed in this study were similar to discrepancies observed in a number of other spaceborne cross-calibration studies.

Keywords: flares, solar corona, Sun, SMART-1, XSM, X-rays, cross-calibration, RHESSI, GOES

1. Introduction

Spaceborne instruments have been cross-calibrated in the past, and for example Maiz-Apellaniz (2005) has cross-calibrated *Tycho-2* (Hog *et al.*, 2000) photometry from ESA's *Hipparcos* and *Hubble Space Telescope Spectrophotometry* (Turnshek *et al.*, 1990). In some cases cross-calibration is taken to mean a calibration with a standard candle, such as the Crab Nebula, as is the case for *International Gamma-Ray Astrophysical Laboratory* (INTEGRAL; Winkler *et al.*, 2003 by Lubinski *et al.* (2004). Occasionally one also sees the cross-calibration of different instruments on the same mission, as is the case for *XMM-Newton* (Jansen *et al.*, 2001) by Kirsch *et al.* (2004).

The situation was similar for the solar instrument *Solar and Heliospheric Observatory* (SOHO) described by Domingo, Fleck, and Poland (1995) when *Coronal Diagnostic Spectrometer* (CDS) and *Solar Ultraviolet Measurements of Emitted Radiation* (SUMER) were intercalibrated in Pauluhn *et al.* (2002). For the

Observatory, P.O. Box 14 FIN-00014 University of Helsinki,
Finland email: mikko.vaananen@helsinki.fi

solar instrument *Extreme ultraviolet Imaging Telescope* (EIT) and CDS-NIS onboard SOHO a sophisticated cross-calibration was recently done with *Transition Region and Coronal Explorer* (TRACE; Handy *et al.*, 1999) by Brooks and Warren (2006). In this cross-calibration the different 171 Å, 195 Å, and 284 Å channel fluxes were compared with predicted count rates generated from a *Differential Emission Measure* (DEM) distribution derived from CDS spectral line intensities. The DEM was convolved with EIT and TRACE temperature response functions, which were calculated with the latest atomic data from the CHIANTI database (Dere *et al.*, 1997) (http://www.ukssdc.ac.uk/solar/chianti/), (Landi *et al.*, 2006), to predict count rates in their observing channels.

Stepnik *et al.* (2003) presents a cross-calibration where *PROgramme National d'AstrOnomie Submillimetrique* (PRONAOS; Serra *et al.*, 2002), a stratospheric balloon-borne submillimetre instrument was cross-calibrated with the ISOPHOT photo-polarimeter of Lemke *et al.* (1996) onboard ESA's *Infrared Space Observatory* (ISO; Kessler *et al.*, 1996) and *Diffuse Infrared Background Experiment* DIRBE onboard NASA's *Cosmic Background Explorer* COBE described for example in Boggess *et al.* (1992).

The current paper presents two sets of cross-calibrations, a model-independent calibration and a Mewe model (Mewe 1985) dependent one. The Mewe model was chosen over the CHIANTI because the Mewe model was provided in all data analysis software systems of all instruments.

Small Missions for Advanced Research and Technology (SMART-1; Foing, *et al.*, 2003) was launched on 27 September 2003, and *X-ray Solar Monitor* (XSM; Huovelin *et al.*, 2002) is the only instrument on SMART-1 for direct observations of the Sun. *Reuven Ramaty High Energy Solar Spectroscopic Imager* (RHESSI; Lin *et al.*, 2002) is a NASA mission launched in 2002 designed to investigate particle acceleration and energy release in solar flares. *Geostationary Operational Environmental Satellite* (GOES; Thomas, Crannell and Starr, 1985) is a constellation of weather satellites, where each GOES satellite carries also a solar X-ray sensor. The XSM spectral range overlaps with GOES and RHESSI. Concurrent events have been observed and the thrust of this paper is to cross-calibrate the instruments with these events. A further objective of this paper is to develop an understanding of the differences found.

2. Cross-Calibration Methods

2.1. XSM Ground and Inflight Calibrations

XSM itself has been calibrated on the ground. Laboratory calibrations of XSM are explained in Alha *et al.* (2008), and the radiation hardness of XSM and the inflight degradation due to space radiation have been studied by Laukkanen *et al.* (2005). XSM is equipped with an inflight spectral calibration source attached to the inner surface of a tungsten shutter. The calibration source consists of ^{55}Fe that is coated with a 5 μm Ti foil and produces emission lines at 4.508 and 4.932 keV (Ti) and 5.895 and 6.492 keV (Mn). The inflight calibration process is also explained in Alha *et al.* (2008).

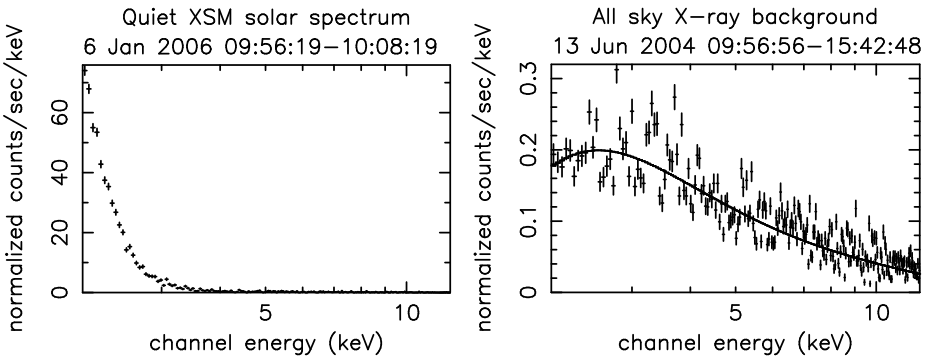

Figure 1. The XSM quiescent solar spectrum on 6 January 2006 09:56:19 – 10:08:19 on the left. The non-solar all sky background on 13 June 2004 09:56:56 – 15:42:48 on the right. The line in the right plot is the fitted cutoff powerlaw.

2.2. Background Subtraction

Background subtraction of XSM data is done based on measured quiescent Sun background spectra integrated over long time periods. Figure 1 shows the quiescent solar spectrum on 6 January 2006 on the left and all sky background spectrum on the right. The flux values derived from these spectra are used in this article when mentioned. Dynamic background subtraction is not possible for all the flares, because not all observations comprise pre- or post flare measurements.

The background flux values deduced from the quiescent solar spectrum were 2.7×10^{-8} W m^{-2} for 1.55 – 12.40 keV and 1.0×10^{-10} W m^{-2} for 6 – 8 keV. The all sky background flux values deduced from the spectrum were 1.0×10^{-9} W m^{-2} for 1.55 – 12.40 keV and 1.7×10^{-10} W m^{-2} for 6 – 8 keV fitted with a cutoff powerlaw between 2 – 12.4 keV.

2.3. XSM and GOES Model-Independent Calibrations

The XSM flux $F_{\rm XSM}$ was derived from XSPEC (Arnaud, 1996) (http://heasarc.gsfc.nasa.gov/docs/xanadu/xspec/) spectral fits that sampled the data best. We used one-minute GOES data $F_{\rm GOES}$ and 16-second XSM data to derive the flux values listed in Table 1. We interpolated XSM measurements to match with the GOES measurements in time with one second accuracy.

We are quoting the σ error derived in this way for the errors, unless otherwise stated.

2.4. XSM and GOES Mewe-Model Calibrations

In addition to the actual flux calibration we obtained the GOES total emission measures (TEM), $\mathrm{TEM_{GOES}}$ and temperatures (T), $T_{\rm GOES}$ using the Mewe model of Mewe (1985) with Meyer abundances (Meyer, 1985) from the GOES routine in SolarSoft (Freeland and Handy, 1998) (http://www.lmsal.com/solarsoft/index_old.html). We fitted the Mewe model to XSM data in XSPEC using the "mekal" algorithm from 2.0 keV onwards to obtain the corresponding $\mathrm{TEM_{XSM}}$, $T_{\rm XSM}$ and $F_{\rm XSM}^{\rm Mewe}$

values. The band between 1.55 – 2.0 keV needs to be extrapolated due to limitations cited in Alha *et al.* (2008). We then compared the Mewe model-generated fluxes $F_{\rm XSM}^{\rm Mewe}$ and $F_{\rm GOES}^{\rm Mewe}$, which we obtain by feeding the GOES routine values from Solarsoft to "mekal" in XSPEC through the XSM response. TEM and T refer to the Mewe generated values for both instruments in XSM-GOES calibrations of this paper. Mewe generated fluxes (F) are mentioned explicitly for both instruments.

The results of these calibrations are discussed in Sections 3.1 and 3.2 and the first conclusion in Section 5.

2.5. XSM and RHESSI

XSM and RHESSI were cross-calibrated in the 6 – 8 keV band. This is the band where the sensitivities of the two instruments are most similar (B. Dennis, H. Hudson, private communication, 7-11 Jun 2005).

The dynamic pre- and postflare background was subtracted for RHESSI. The quiescent XSM background was subtracted for XSM. XSM fluxes were calculated by fitting the vRaymond (Raymond and Smith, 1977) + broken powerlaw model between 5 – 10 keV in XSPEC and "vth" using the Mewe full model in OSPEX (http://hesperia.gsfc.nasa.gov/ssw/packages/spex/doc/ospex_explanation.htm) of Solarsoft (Freeland and Handy, 1998) was used to derive RHESSI fluxes. XSM data was also fed into OSPEX, and the two models produced the same flux results independently in both XSPEC and OSPEX. Therefore any differences in software or model methodology are ruled out as sources of discrepancy.

3. Cross-Calibration Results

In the following we describe the cross-calibration results obtained from each pair of instruments individually.

3.1. XSM and GOES Model-Independent Calibrations

The light curves of Figure 2 demonstrate that XSM and GOES are working coherently in time.

Table 1 provides a comprehensive list of all model-independent XSM-GOES flux calibrations performed in chronological order. Table 1 also displays the XSM/GOES flux ratios and their errors. The flux ratio is between 1.23 and 0.69. The average flux ratio is 0.94 ± 0.09. $\theta_{\rm XSM}^{\rm off-axis}$ is the angle between the Sun and the optical axis of XSM.

In the top plot of Figure 3 the $F_{\rm XSM}/F_{\rm GOES}$ ratio is plotted as a function of $F_{\rm XSM}$. There appears to be no significant trend in this ratio with $F_{\rm XSM}$. If interval 6, an essentially quiescent interval is omitted, the $F_{\rm XSM}/F_{\rm GOES}$ ratio is also 0.94 ± 0.09.

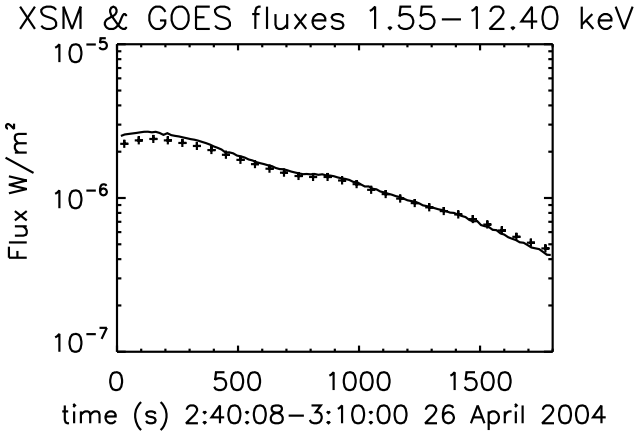

Figure 2. The plot shows both GOES (+signs) 1 – 8 Å and XSM (solid line) light curves on the 26 April 2004 2:40:08 – 3:10:00.

Table 1. Comprehensive calibration list of fluxes of GOES and XSM measured in the 1.55 – 12.40 keV band during one-minute periods in chronological order from April 2004 to April 2005. Errors are the standard deviations of the mean σ.

Interval	time (min)	$F_{\rm GOES}$ (W m^{-2})	$F_{\rm XSM}$ (W m^{-2})	$F_{\rm XSM}/F_{\rm GOES}$	$\theta_{\rm XSM}^{\rm off-axis}$ (deg)
1	03:02 26 Apr 2004	8.22×10^{-7}	$(8.28 \pm 0.37) \times 10^{-7}$	(1.01 ± 0.04)	4
2	19:38 5 May 2004	8.38×10^{-8}	$(7.34 \pm 0.86) \times 10^{-8}$	(0.88 ± 0.12)	13
3	7:30 24 May 2004	3.28×10^{-7}	$(2.90 \pm 0.89) \times 10^{-7}$	(0.88 ± 0.31)	39
4	11:06 24 May 2004	4.47×10^{-6}	$(4.57 \pm 1.16) \times 10^{-6}$	(1.02 ± 0.25)	39
5	05:47 16 Jun 2004	5.65×10^{-7}	$(3.91 \pm 1.05) \times 10^{-7}$	(0.69 ± 0.27)	41
6	20:27 5 Jul 2004	3.43×10^{-8}	$(3.29 \pm 0.79) \times 10^{-8}$	(0.96 ± 0.24)	14
7	05:31 31 Jul 2004	4.14×10^{-7}	$(3.93 \pm 0.02) \times 10^{-7}$	(0.95 ± 0.01)	17
8	05:27 25 Aug 2004	7.01×10^{-7}	$(6.19 \pm 0.64) \times 10^{-7}$	(0.88 ± 0.10)	12
9	05:59 15 Jan 2005	7.34×10^{-6}	$(9.00 \pm 1.13) \times 10^{-6}$	(1.23 ± 0.13)	16
10	12:51 4 Apr 2005	2.90×10^{-7}	$(2.71 \pm 0.10) \times 10^{-7}$	(0.93 ± 0.04)	26

3.2. XSM and GOES Mewe-Model calibrations

Table 2 presents the GOES and XSM fluxes ($F_{\rm GOES}^{\rm Mewe}$, $F_{\rm XSM}^{\rm Mewe}$), TEMs (TEM$_{\rm GOES}$, TEM$_{\rm XSM}$) and temperatures ($T_{\rm GOES}$, $T_{\rm XSM}$) obtained from the Mewe model with Meyer abundances. The average $F_{\rm XSM}^{\rm Mewe}/F_{\rm GOES}^{\rm Mewe}$ ratio is 0.92 ± 0.05, meaning that the GOES response produces the same flux with the Mewe model in comparison to XSM. The average TEM$_{\rm XSM}$/TEM$_{\rm GOES}$ ratio is 1.23 ± 0.08. The XSM temperatures fitted with the Mewe model are about 50% higher; the average $T_{\rm XSM}/T_{\rm GOES}$ ratio equals 1.47 ± 0.03.

As we can see from Table 2 and Figure 3, interval 6 deviates quite far from the general trend in Figure 3. This is because it is essentially a quiescent interval. In this quiet state the $F_{\rm XSM}^{\rm Mewe}/F_{\rm GOES}^{\rm Mewe}$ ratio is 1.30 ± 0.09, $T_{\rm XSM}/T_{\rm GOES}$ ratio is 0.60 ± 0.02 and the TEM$_{\rm XSM}$/TEM$_{\rm GOES}$ ratio is 8.07 ± 0.1.

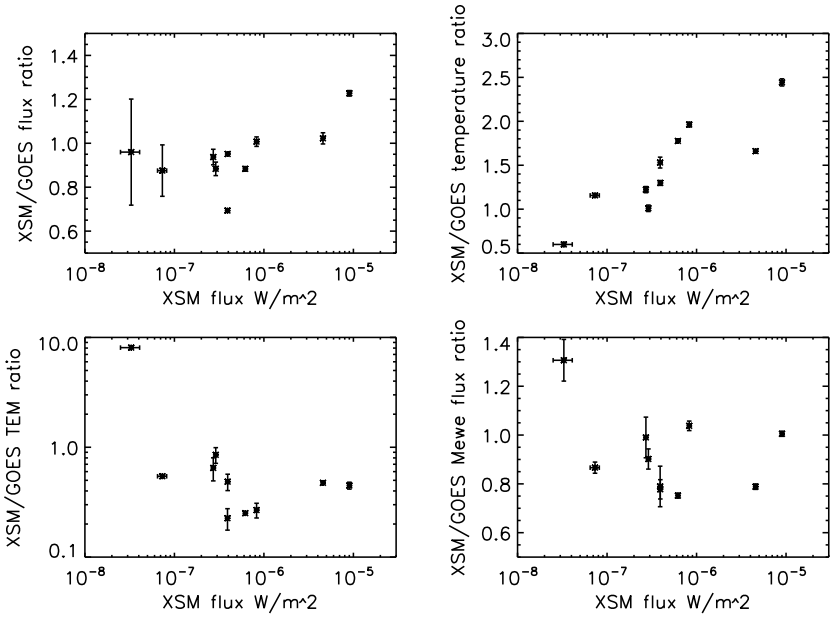

Figure 3. $F_{\rm XSM}/F_{\rm GOES}$ ratios plotted as a function of XSM flux (Table 1) on top left. On top right the $T_{\rm XSM}/T_{\rm GOES}$ plotted as a function of XSM flux. On bottom left the $\rm TEM_{XSM}/TEM_{GOES}$ is plotted as a function of XSM flux. On bottom right $F^{\rm Mewe}_{\rm XSM}/F^{\rm Mewe}_{\rm GOES}$ is plotted as a function of XSM flux. Interval 6 is the lowest point in top right plot and highest point in lower-left plot.

Table 2. Events of Table 1 calibrated using the Mewe (1985) model with Meyer (1985) abundances for both XSM and GOES data.

Interval	$T_{\rm GOES}$ (keV)	$T_{\rm XSM}$ (keV)	$\rm TEM_{GOES}$ ($10^{47}\rm cm^{-3}$)	$\rm TEM_{XSM}$ ($10^{47}\rm cm^{-3}$)	$F^{\rm Mewe}_{\rm GOES}$ (W $\rm m^{-2}$)	$F^{\rm Mewe}_{\rm XSM}$ (W $\rm m^{-2}$)
1	0.48	0.94 ± 0.01	40	10.8 ± 0.2	8.83×10^{-7}	$(9.20 \pm 0.14) \times 10^{-7}$
2	0.37	0.42 ± 0.01	13	7.1 ± 0.1	1.23×10^{-7}	$(1.07 \pm 0.03) \times 10^{-7}$
3	0.52	0.53 ± 0.02	17	14.4 ± 2.0	4.68×10^{-7}	$(4.22 \pm 0.17) \times 10^{-7}$
4	0.94	1.56 ± 0.02	75	35.6 ± 0.5	6.39×10^{-6}	$(5.04 \pm 0.06) \times 10^{-6}$
5	0.39	0.60 ± 0.04	65	14.6 ± 2.8	7.40×10^{-7}	$(5.84 \pm 0.49) \times 10^{-7}$
6	0.47	0.28 ± 0.01	2.5	20.1 ± 2.1	5.19×10^{-8}	$(6.78 \pm 0.58) \times 10^{-8}$
7	0.62	0.80 ± 0.02	15	7.2 ± 0.3	6.33×10^{-7}	$(4.92 \pm 0.19) \times 10^{-7}$
8	0.53	0.95 ± 0.01	35	8.8 ± 0.1	1.01×10^{-6}	$(7.59 \pm 0.08) \times 10^{-7}$
9	1.27	3.10 ± 0.13	80	35.8 ± 1.2	9.32×10^{-6}	$(9.36 \pm 0.27) \times 10^{-6}$
10	0.60	0.74 ± 0.03	10	6.5 ± 0.6	3.92×10^{-7}	$(3.88 \pm 0.32) \times 10^{-7}$

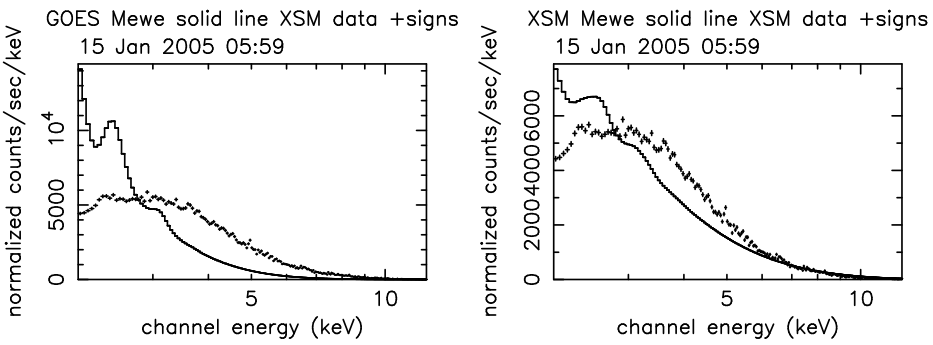

Figure 4. The Mewe emission spectra predicted by GOES (left) and XSM (right) is plotted as a solid line, XSM data marked by + signs. The event is the largest flare, interval number 9.

If the quiescent interval 6 is discounted from the averages to obtain pure "flare-on" values, the average $F_{\rm XSM}^{\rm Mewe}/F_{\rm GOES}^{\rm Mewe}$ ratio is 0.88 ± 0.05, the average $T_{\rm XSM}/T_{\rm GOES}$ ratio is 1.56 ± 0.03 and the average $\rm TEM_{XSM}/TEM_{GOES}$ ratio is 0.46 ± 0.08.

Figure 3 shows that the $T_{\rm XSM}/T_{\rm GOES}$ increases as a function of $F_{\rm XSM}$. As for the bottom plots, neither $F_{\rm XSM}^{\rm Mewe}/F_{\rm GOES}^{\rm Mewe}$ or $\rm TEM_{XSM}/TEM_{GOES}$ seem to vary with $F_{\rm XSM}$.

It should also be noted that towards the higher energy flares the observed spectrum deviates more from the Mewe model. In order to visualise the situation, the Mewe models predicted by GOES and XSM are plotted against XSM data for interval 9, the biggest flare, in Figure 4. The spectral model could be improved with the addition of a high-energy component.

3.3. XSM and RHESSI

Figure 5 displays a longer duration light curve from the decay phase of the same flare as in Figure 1.

The average flux ratio of XSM flux/RHESSI flux between 6 – 8 keV was 2.63. Similar measurement errors as in the previous section put the ratio at 2.63 ± 0.23, assuming XSM errors only. At lower flux levels, the measurements approach each other. The flux ratio is steady around the average at the beginning of the interval, but varies quite randomly between 0.6 to 10 at the end of the measurement interval.

4. Discussion

The flux differences between GOES and XSM appear to be within the measurement error. Half of the calibrations have $F_{\rm GOES}$ and $F_{\rm XSM}$ within σ, and 9/10 intervals are within $3\,\sigma$. When the Mewe model and Meyer abundances were used with both XSM and GOES data, $T_{\rm XSM}$ was 1.47 ± 0.03 times higher than $T_{\rm GOES}$. In contrast, $F_{\rm XSM}^{\rm Mewe}$ was 0.92 ± 0.05 times lower than $F_{\rm GOES}^{\rm Mewe}$ and $\rm TEM_{XSM}$ was 1.23 ± 0.08 times higher than $\rm TEM_{GOES}$. We believe that the likely cause for the

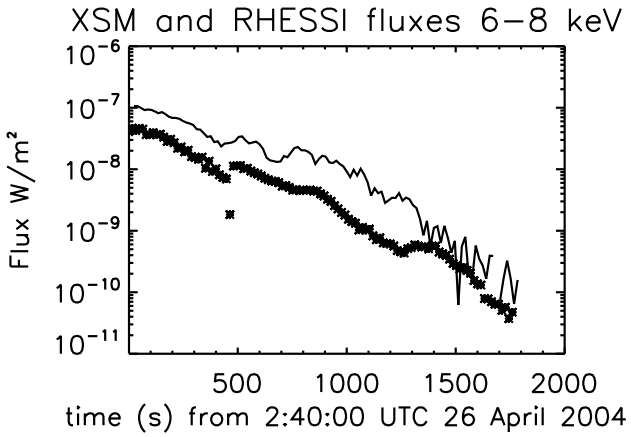

Figure 5. RHESSI and XSM fluxes plotted as a function of time in the 6 – 8 keV band. XSM flux is the solid line, RHESSI flux is marked by crosses.

discrepancy between XSM and GOES in the Mewe model derived parameters relates to three factors:

i) The statistics of the data: GOES has only two, whereas XSM has 512 channels.

ii) Extrapolation of XSM data between 1.55 – 2.0 keV from a fit between 2.0 – 12.4 keV to overcome the practical low energy limitations of XSM as explained in Alha *et al.* (2008).

iii) The need for a high-energy spectral component.

The Mewe model is a thermal line emission + continuum model. Figure 4 clearly shows that this model is not as appropriate for estimating the flux, T or TEM with bigger flares, as may the case be with quiescent solar observations or small flares. The Mewe model misses an important part of the high energy flux, which probably has a non-thermal origin. In order to improve upon the predictability of model parameters from GOES data it is probably not enough to update the line emission model only, to say CHIANTI for example, as has been done in OSPEX. The GOES differences in temperature and emission measure responses observed with different models of Mewe and CHIANTI in White, Thomas, and Schwartz (2005) are about 25%, and would suggest that a change in the emission model might compensate for some discrepancies. Based on the observations made here, the calibration should be repeated with CHIANTI and XSM data in the future.

The XSM/RHESSI flux ratio is 2.63 ± 0.23, where the error derives solely from the estimated error for XSM. In order to bring the measurements to within 3 σ of each other the relative RHESSI flux error should be σ=0.33. This σ may be possible, but in addition there could be systematic effects that amount to the discrepancy observed. Firstly, it should be noted that between 5 – 10 keV the effective area of RHESSI falls over two orders of magnitude as noted in Smith *et al.* (2002), so defining the effective area is difficult. In this same band the XSM effective area varies by less than 5 % as explained in Huovelin *et al.* (2002).

During the calibration interval at approximately 26 April 2004 02:48 RHESSI changes from A1 state (=thin attenuator on) to A0 state where no attenuators are on. It is probably this event that causes the one single dropped data point in Figure 5 at approximately 480 seconds. However, considering that the XSM/RHESSI flux ratio behaves normally on both sides of this point, the attenuators are not likely to distort recorded fluxes.

XSM saw a higher photon flux than RHESSI at the higher energies. Time integrated average spectra of this interval revealed that the flux was 2.6×10^{-8} W m^{-2} between 6.0 – 8.0 keV averaged over the entire observation period. This is two orders of magnitude higher than quiescent background or all sky background (both about 1×10^{-10} W m^{-2}) during a GOES B-class flare. Therefore there is reason to believe this flux is solar in origin.

In order to put these calibration results into perspective they could perhaps be compared with Brooks and Warren (2006) where a discrepancy of 3 – 25% was observed when CDS DEMs were used to predict TRACE and EIT 171 Å and 195 Å count rates and the two-to-five fold discrepancy was observed for the 284 Å count rate. In Stepnik *et al.* (2003) a 0.7 conversion coefficient was obtained between ISOPHOT and PRONAOS. For the Ne VIII narrow line observation at 77.0 nm (Pauluhn *et al.*, 2002) reported an average ratio of 2.6 for the CDS-GIS-4 to SUMER radiances, when CDS measured 30% higher values than SUMER for the He I line at 58.4 nm. Remarkably the narrow band calibrations conducted between XSM and RHESSI show discrepancies similar to those observed by Pauluhn *et al.* (2002) for SUMER and CDS-GIS-4 detector, or the 284 Å channel of TRACE and EIT in Brooks and Warren (2006). The flux calibration between XSM and GOES shows discrepancies that are smaller or similar to the discrepancies observed in the cross-calibrations of Brooks and Warren (2006) for the other channels and Stepnik *et al.* (2003) and Pauluhn *et al.* (2002) for the He I line.

5. Conclusions

The main conclusions reached in these cross-calibrations were:

i) The model independent $F_{\rm XSM}/F_{\rm GOES}$ ratio is 0.94 ± 0.09 for data prior to April 2005. XSM and GOES agree in terms of model independent and Mewe model dependent fluxes. However, discrepancies arise in the model parameters T and TEM predicted by the Mewe model with Meyer abundances. It is suggested that the discrepancies arise from three factors, first of which is the lack of sampling due to the GOES data having only two channels in contrast to 512 channels for XSM. The second is the extrapolation of the model between 1.55 – 2.0 keV in the $F_{\rm XSM}^{\rm Mewe}$. The third suggested source for discrepancy is an additional high-energy component in the spectral model.

ii) The average XSM/RHESSI flux ratio is 2.63 ± 0.23. There are a number of possible sources for discrepancy, one of which is that within the calibration band of 6 – 8 keV an asymptotic change in RHESSI effective area introduces error.

iii) The calibration results discovered here are similar to results obtained from other spaceborne cross-calibrations from Brooks and Warren (2006), Pauluhn *et al.* (2002) and Stepnik *et al.* (2003).

Acknowledgements This work was made possible by ESA staff and other instrument teams involved in the SMART-1 mission. We also thank Dr Bernard Foing at ESA and Dr Manuel Grande in the UK. Acknowledgements are due for the entire RHESSI -team for their assistance. In particular we extend our thanks to Drs Brian Dennis, Richard Schwartz, Kim Tolbert GSFC/NASA and Hugh Hudson, Gordon Hurford, Robert Lin and Jim McTiernan of Space Sciences Lab at University of California at Berkeley and Ken Phillips at Mullard Space Sciences Laboratory, UK. Dr. Jukka Nevalainen is acknowledged for advice that improved the manuscript. This work was funded by the following grants: Väisälä foundation PhD grants, Academy of Finland research grants 74882 and 211061 and Suinno Oy. The anonymous referee is acknowledged for suggesting several improvements and clarifying the paper.

References

Alha, L., Huovelin, J., Hackman, T., Andersson, H., Howe, C.J., Esko, E., Väänänen M.K.: 2008, The in-flight performance of the X-ray Solar Monitor (XSM) on-board SMART-1. *Nuc. Instr. Methods* **596**, 317.

Arnaud, K.A.: 1996, XSPEC: The First Ten Years. In: Jacoby, G.H., Barnes, J.(eds.) *Astronomical Data Analysis Software and Systems V*, **CS-100**, Astron. Soc. Pac., San Francisco, 17.

Boggess, N.W., Mather, J.C., Weiss, R., Bennett, C.L., Cheng, E.S., Dwek, E., Gulkis, S., Hauser, M.G., Janssen, M.A., Kelsall, T., *et al.*: 1992, The COBE Mission: Its Design and Performance Two Years After Launch. *Astrophys. J.* **397**, 420.

Brooks, D.H., Warren, H.P.: 2006, The Intercalibration of SOHO EIT, CDS-NIS, and TRACE. *Astrophys. J.* **164**, 202.

Dere, K.P., Landi, E., Mason, H.E., Monsignori Fossi, B.C., Young, P.R.: 1997, CHIANTI - an atomic database for emission lines. *Astron. Astrophys. Suppl. Ser.* **125**, 149.

Domingo, V., Fleck, B., Poland, A.I.: 1995, The SOHO Mission: an Overview. *Solar Phys.* **162**, 1.

Foing, B.H., Racca, G.D., Marini, A., Heather, D.J., Koschny, D., Grande, M., Huovelin, J., Keller, H.U., Nathues, A., Josset, J.L., *et al.*: 2003, SMART-1 mission to the moon: Technology and science goals. *Adv. Space Res.* **31**, 11, 2323.

Freeland, S.L., Handy, B.N.: 1998, Data Analysis with the SolarSoft System. *Solar Phys.* **182**, 2, 497.

Handy, B.N., Acton, L.W., Kankelborg, C.C., Wolfson, C.J., Akin, D.J., Bruner, M.E., Caravalho, R., Catura, R.C., Chevalier, R., Duncan, D.W. *et al.*: 1999, The Transition Region and Coronal Explorer. *Solar Phys.* **187**, 229.

Hog, E., Fabricius, C., Makarov, V.V., Urban, S., Corbin, T., Wycoff, G., Bastian, U., Schwekendiek, P., Wicenec, A. *et al.*: 2000, The Tycho-2 Catalogue of the 2.5 million brightest stars. *Astron. Astrophys.* **355**, 27.

Huovelin, J., Alha, L., Andersson, H., Andersson, T., Browning, R., Drummond, D., Foing, B., Grande, M., Hämäläinen, K., Laukkanen, J. *et al.*: 2002, The SMART-1 X-ray solar monitor (XSM): calibrations for D-CIXS and independent coronal science. *Planet. Space Sci.* **50**, 1345.

Jansen, F., Lumb, D., Altieri, B., Clavel, J., Ehle, M., Erd, C., Gabriel, C., Guainazzi, M., Gondoin, P., Much, R. *et al.*: 2001, XMM-Newton observatory. I. The spacecraft and operations. *Astron. Astrophys.* **365**, 1.

Kessler, M.F., Steinz, J.A., Anderegg, M.E., Clavel, J., Drechsel, G., Estaria, P., Faelker, J., Riedinger, J.R., Robson, A., Taylor, B.G., Ximenez de Ferran, S.: 1996, The Infrared Space Observatory (ISO) Mission. *Astron. Astrophys.* **315**, 27.

Kirsch, M.G.F., Altieri, B., Chen, B., Haberl, F., Metcalfe, L., Pollock, A.M.T., Read, A.M., Saxton, R.D., Sembay, S., Smith, M.J.S.: 2004, XMM-Newton (cross)-calibration. *SPIE* **5488**, 103.

Landi, E., Del Zanna, G., Young, P.R., Dere, K.P., Mason, H.M., Landini, M.: 2006, CHIANTI -An Atomic Database for Emission Lines. VII. New Data for X-rays and Other Improvements. *Astrophys. J. Suppl. Ser.* **162**, 261.

Laukkanen, J., Lämsä, V., Salminen, A., Huovelin, J., Andersson, H., Alha, L., Hämäläinen, K., Nenonen, S., Sipilä, H., Tillander, M.: 2005, Radiation hardness studies for the X-ray Solar Monitor (XSM) onboard the ESA SMART-1 mission. *Nuc. Instrum. Methods in Phys Res Section A* **538**, 1-3, 496.

Lemke, D., Klaas, U., Abolins, J., Abraham, P., Acosta-Pulido, J., Bogun, S., Castaneda, H., Cornwall, L., Drury, L., Gabriel, C. *et al.*: 1996, ISOPHOT -capabilities and performance. *Astron. Astrophys.* **315**, 64.

Lin, R.P., Dennis, B.R., Hurford, G.J., Smith, D.M., Zehnder, A., Harvey, P.R., Curtis, D.W., Pankow, D., Turin, P., Bester, M. *et al.*: 2002, The Reuven Ramaty High-Energy Solar Spectroscopic Imager (RHESSI). *Solar Phys.* **210**, 3.

Lubinski, P., Dubath, P., Kretschmar, P., Pottschmidt, K., Walker, R.: 2004, Integral Cross-Calibration Status. *Proc. 5th INTEGRAL Science Workshop* **SP-552**, ESA Noordwijk 871.

Maiz-Apellaniz, J.: 2005, A Cross-Calibration between Tycho-2 Photometry and Hubble Space Telescope Spectrophotometry. *Pub. Astronom. Soc. Pacific* **117**, 615.

Mewe, R., Gronenschild, E.H.B.M., van den Oord, G.H.J.: 1985, Calculated X-radiation from optically thin plasmas. *Astron. Astrophys. Suppl. Ser.* **62**, 197.

Meyer, J.P.: 1985, Solar-Stellar Outer Atmospheres and Energetic Particles, and Galactic Cosmic Rays. *Astrophys. J. Suppl. Ser.* **57**, 173.

Pauluhn, A., Lang, J., Schühle, U., Solanki, S.K., Wilhelm, K., Pike, C.D., Thompson, W.T., Rüedi, I., Hollandt, J., Huber, M.C.E. : 2002, Intercalibration of CDS and SUMER. *Proc. SOHO 11 Symposium, From Solar Min to Max:Half a Solar Cycle with SOHO* **SP-508**, ESA Nordwijk, 223.

Raymond, J.C., Smith, B.W.: 1977, Soft X-ray spectrum of a hot plasma. *Astrophys. J. Suppl. Ser.* **35**, 419.

Serra, G., Giard, M., Bouchou, F., Dupac, X., Gabarrot, F., Meny, C., Ristorcelli, I., Lamarre, J.M., Bernard, J.P., Pajot, F. *et al.*: 2002, PRONAOS: Two Meter Submillimeter Balloon Borne Telescope. *Adv. Space Res.* **30**, 1297.

Smith, D.M., Lin, R.P., Turin, P., Curtis, D.W., Primbsch, J.H., Campbell, R.D., Abiad, R., Schroeder, P., Cork, C.P., Hull, E.L. *et al.*: 2002, The RHESSI Spectrometer. *Solar Phys.* **210**, 33.

Stepnik, B., Pajot, F., Lamarre, J.-M., Abergel, A., Bernard, J.-P., Giar,d M., Meny, C., Ristorcelli, I., Serra, G., Torre, J.-P.: 2003, Cross-Calibration of PRONAOS and ISO. *Proceedings The Calibration Legacy of the ISO Mission*, **SP-481**, ESA Nordwijk, 187.

Thomas, R.J., Crannell, C.J., Starr, R.: 1985, Expressions to determine temperatures and emission measures for solar X-ray events from GOES measurements *Solar Phys.* **95**, 323.

Turnshek, D.A., Bohlin, R.C., Williamson, R.L. II, Lupie, O.L., Koornneef, J., Morgan, D.H.: 1990, An Atlas of Hubble Space Telescope Photometric, Spectrophotometric, and Polarimetric Calibration Objects. *Astron. J.* **99**, 1243.

White, S.M., Thomas, R.J., Schwartz, R.A.: 2005, Updated Expressions for Determining Temperatures and Emission Measures from GOES Soft X-ray Measurements. Solar Phys. **227**, 231.

Winkler, C., Courvoisier, T.J.-L., Di Cocco, G., Gehrels, N. ,Gimenez, A., Grebenev, S., Hermsen, W., Mas-Hesse, J.M., Lebrun, F., Lund, N. *et al.*: 2003, The INTEGRAL mission. *Astron. Astrophys.* **411**, 1.